P3.14 QUANTIFICATION OF A DRY BIAS IN RADIOSONDE HUMIDITY PROFILES OVER ANTARCTICA: IMPLICATIONS FOR CALCULATIONS OF OUTGOING LONGWAVE RADIATION

Penny M. Rowe *[1], Von P. Walden[1], Larry M. Miloshevich[2]
(1) Department of Geography, University of Idaho, Moscow, ID
(2) National Center for Atmospheric Research, Boulder, Colorado

Abstract

Middle to upper tropospheric humidity plays a large role in determining outgoing longwave radiation. Tropospheric humidity is routinely measured by radiosondes, even though radiosonde humidity measurements typically become increasingly inaccurate with height. Among the problems experienced by the humidity sensor is a dry bias caused by illumination with solar radiation. During the austral summer of 2003/2004, at Dome C, Antarctica, Vaisala RS-90 radiosoundings were launched to measure tropospheric pressure, temperature and humidity in clear-sky conditions. During this time, the Polar Atmospheric Emitted Radiance Interferometer (PAERI) measured downwelling spectral infrared radiance at Dome C. The humidity profiles are corrected for a time lag and calibration error and then used to simulate downwelling radiances. The humidity profiles are scaled to obtain best agreement between the measurements and calculations. The mean corrections in absolute humidity are determined to be 8% and 23% for solar zenith angles of about 80° and 60°. Tropospheric pressures above Dome C range from 650 mb to 200 mb. Calculations of the outgoing longwave flux indicate that dry biases of 8% and 23% in middle to upper tropospheric humidity (650 - 200 mb) in the tropics result in overestimating outgoing longwave flux by about 1 W m^{-2} and 3 W m^{-2}.

1. INTRODUCTION

The outgoing longwave radiation (OLR) is very sensitive to atmospheric humidity, since water-vapor is the most important greenhouse gas. The outgoing longwave flux is particularly sensitive to middle and upper tropospheric humidity (M/UTH, 650-250 mb) [see, *e.g.* Sinha *et al.* (1995)]. Thus measurements of M/UTH globally are important for understanding the radiation budget. Furthermore, accurate measurements of upper tropospheric humidity are needed to determine the magnitude of the water-vapor feedback as atmospheric CO_2 increases and, thus, to predict climate change (Buehler *et al.*, 2005 and references therein). Humidity profiles inferred from remote sensing lack fine vertical resolution; Buehler *et al.* (2005) found that OLR can vary by 1 W m^{-2} due to variations in humidity on vertical scales smaller than 4 km.

Radiosonde humidity sensors have high vertical resolution but typically become increasingly inaccurate with height throughout the troposphere. Much work has been done to identify and minimize sources of error (Wang *et al.*, 2002; Miloshevich *et al.*, 2001; 2004; 2006; Turner *et al.*, 2003) in different generations of radiosondes (RS-80, RS-90, and RS-92). RS-90 and RS-92 radiosonde humidity sensors do not have radiation shields to protect them from solar heating. The dry bias caused by solar heating of the sensor arm (hereafter, dry bias) depends on solar angle, altitude, and sensor orientation. A recent study by Vőmel *et al.* (submitted, 2006), found that the dry bias in the Vaisala RS-92 humidity at Alajuela, Costa Rica, increased from about 9% to 50% from 1000 to 200 mb (0-15 km), for solar zenith angles (SZAs) between 10 and 30 degrees.

Because tropospheric pressures at Dome C, Antarctica, are 650 to 200 mb, Dome C can be used to study the dry bias experienced by radiosonde humidity sensors in the middle to upper troposphere at other locations. In this work, we correct RS-90 humidity measurements made in the Dome C atmosphere using measurements of downwelling spectral infrared radiance. The downwelling radiances were measured with the Polar Atmospheric Emitted Radiance Interferometer (PAERI). Radiosonde and PAERI measurements were made concurrently during the austral summer of 2003/2004. The radiosonde pressure, temperature, and humidity profiles were used in simulating downwelling radiance spectra; correction factors for the humidity profiles were determined by comparing measured and simulated radiances. Measurements were made for SZAs near 60 and 80 degrees. We compare our dry-bias correction for SZAs near 60 degrees to the height-dependent correction of Vőmel *et al.* (submitted, 2006) for SZAs between 10 and 30 degrees. Finally, we calculate the errors such dry biases would induce in the tropical OLR.

2. DATA

Vaisala RS-90 radiosondes were used to measure atmospheric temperature, pressure, and humidity. Errors in humidity due to thermal shock were eliminated through careful radiosonde storage and launch procedures [see the suggestions of Hudson *et al.* (2004)].

* *Corresponding author address:* Penny M. Rowe, 1515 N. Prospect St., Tacoma, WA 98406; e-mail: prowe@harbornet.com

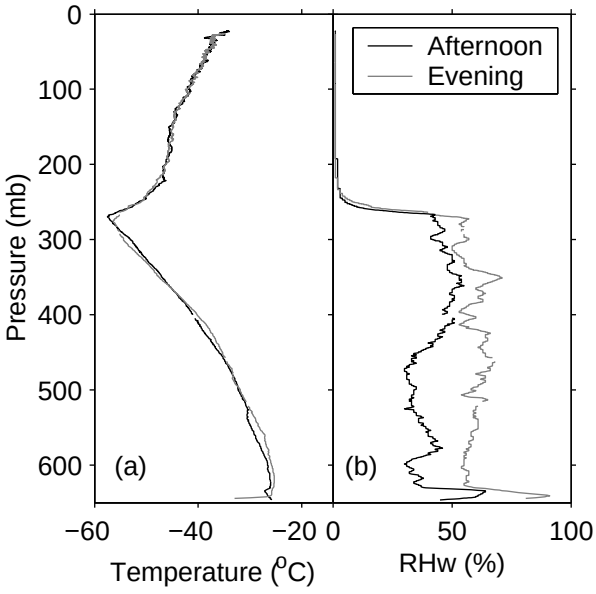

FIG. 1: Profiles of (a) temperature and (b) relative humidity with respect to water (RHw) measured by a Vaisala RS-90 radiosonde at Dome C on 13 January 2004 during the afternoon (15.4 local time) and evening (23.6 local time).

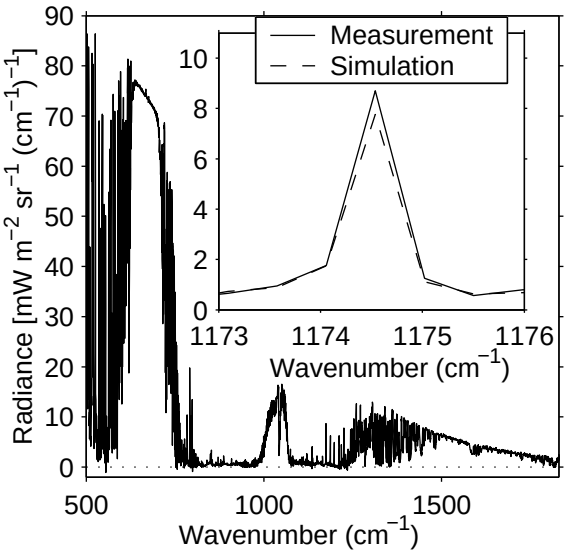

FIG. 2: A downwelling radiance spectrum measured at Dome C in the afternoon (13 January 2004 15.2-16.6 local time). The inset panel shows the radiance for a single water-vapor line from both the measurement and a simulated spectrum.

The method of Miloshevich *et al.* (2004) was used to correct for the response time of the humidity sensor. The low temperature calibration correction of Miloshevich *et al.* (2006) was applied. Radiosonde measurements were made during the afternoon (around 16 LT; LT = Local Time = GMT+8), when SZAs were close to 60 degrees, and during the late evening (around 24 LT), when SZAs were near 80 degrees. Figure 1 shows the temperature and humidity measured on 13 January 2004 during the afternoon and late evening. In Fig. 1a, we see that the temperature profiles are almost identical except at the surface. By contrast, radiosonde humidities differ markedly; humidities are much lower in the afternoon than in the evening (Fig. 1b), consistent with a dry bias caused by solar heating of the sensor. These radiosoundings were fairly typical of those launched during this field season and will serve as the afternoon and evening case studies.

The PAERI measured downwelling infrared radiance in the spectral region between 500 and 2200 cm^{-1} at 1 wavenumber resolution, for a zenith view. Spectra were comprised of 20-90 coadds. Between 2 and 13 spectra were taken over the duration of each radiosounding; these were averaged. PAERI measurements made concurrently with radiosoundings under clear skies were selected for this study. To verify the absence of hydrometeors, the measured downwelling radiance at 961 cm^{-1} was used. This frequency is sensitive to hydrometeors but is fairly insensitive to trace gases: average radiances between 0 and 0.4 RU were assumed to indicate clear skies. The PAERI is described in detail in Rowe *et al.* (2006, *in press*) and Knuteson *et al.* (2004a,b).

The Line-By-Line Radiative Transfer Model (LBLRTM; Clough *et al.*, 1991) was used to simulate downwelling radiances, using radiosonde profiles as input. Lineshape parameters were taken from the HITRAN database (Rothman *et al.*, 2004). The humidity was set to 5 ppmv from about 8 to 24 km above the surface, and to 4 ppmv from 24 to 60 km, in keeping with the suggestion of Walden *et al.* (1998). The temperature profile above the sounding was determined from the South Polar model atmosphere for January developed by Walden *et al.* (1998). For profiles of N_2O, CH_4, O_3, CO_2, and CFCs, measurements made at the surface at South Pole Station over various austral summers were used (NOAA-CMDL; Duglokencky *et al.*, 1998; Conway *et al.*, 1994; and Novelli *et al.*, 1991). For other trace gases, the subarctic-winter standard atmosphere of McClatchey *et al.* (1972) was used.

A measured downwelling radiance spectrum for the afternoon case study is shown in Fig. 2. The inset plot shows an expanded view of a strong water-vapor line for both the measured downwelling radiance and a simulated spectrum. Note that the simulated radiance in the inset plot is lower than the measured radiance close to the line center; this was generally true for all measured radiances near the centers of strong water-vapor lines. Increasing the water-vapor amount at all heights can typically increase the simulated radiance, bringing it into agreement with the measured radiance.

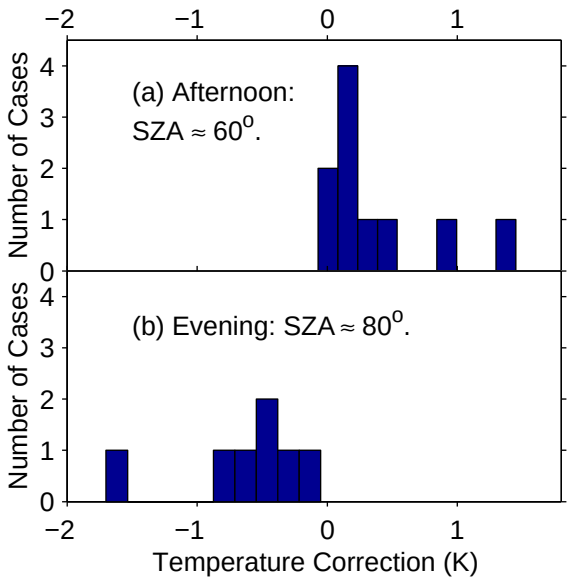

FIG. 3: Temperature Corrections retrieved in the lowest 60 m for (a) afternoon and (b) evening datasets. Measurements were made during the austral summer of 2003/2004 at Dome C. SZA is the solar zenith angle.

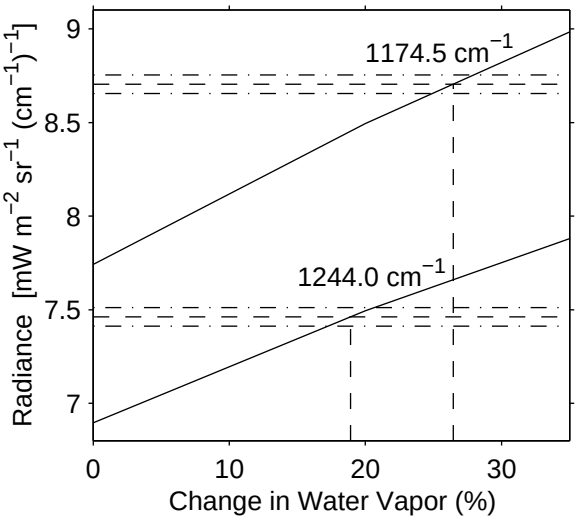

FIG. 4: The simulated downwelling radiance as a function of change in atmospheric water vapor (solid lines) and the measured downwelling radiances (dashed lines) ± one standard deviation (dot-dashed lines), at two different frequencies near the centers of strong lines of water vapor. The radiosounding and downwelling radiance measurement were performed on 13 January 2004 at 15.4 local time at Dome C.

3. METHODS

3.1 *Temperature Correction*

Like the humidity sensor, the temperature sensor is subject to errors that typically worsen with altitude. The temperature was corrected in a height-dependent manner by modifying the temperature profile to decrease the difference between measured and simulated radiances in the CO_2 band from 650 to 760 cm^{-1}, using constrained linear inversion (Rowe, 2004; Rowe *et al.*, 2006, *in press*).

The temperature corrections within the first 60 m are summarized in Fig. 3a for all afternoon cases and in Fig. 3b for all evening cases. In the afternoon, the surface temperature correction is generally positive, but in the evening it is negative. Corrections above 60 m were small except for 200-1500 m, where there was strong disagreement between simulated and measured radiances from 715 to 725 cm^{-1}. The disagreements were very similar for all cases, suggesting that they might be due to inaccuracies in the CO_2 lineshape parameters.

3.2 *WATER-VAPOR CORRECTIONS*

A height-dependent water-vapor retrieval was attempted. Kernels for the constrained linear inversion K were created numerically for frequencies i near strong lines of water vapor, so that the measured-minus-simulated radiance g_i is

$$g_i = \int K_i(x) f(x) dx, \qquad (1)$$

where x is the altitude and f(x) is a change in water vapor. From principal component analysis it was determined that there is only one unique kernel (the singular values that characterize the set of kernels were compared to the experimental uncertainty). Thus water-vapor cannot be retrieved in a height-dependent way.

Rather than a height-dependent water-vapor retrieval, the water-vapor amount is scaled by a single factor at all heights. This is akin to scaling relative humidity to match the total precipitable water vapor measured with microwave instruments (Turner *et al.*, 2003). We scale the water-vapor amount until we achieve the best agreement between the measured downwelling radiance and simulations using the scaled water-vapor profile, at frequencies near strong line centers within 1100-1300 cm^{-1}. This spectral region was chosen because the water-vapor continuum is negligible here for these atmospheric conditions.

To understand the method, it is helpful to see how the simulated radiance changes with water-vapor amount at a single frequency, as shown in Fig. 4. The change in water vapor at the intersection between simulated radiances (solid lines) and measured radiances (horizontal dashed lines) is different for the two different frequencies because the errors are different at these frequencies. To determine the water-vapor correction, we minimized the RMS difference between measured and simulated radiances for the set of frequencies close to strong line-centers of water vapor, as shown in Fig. 5.

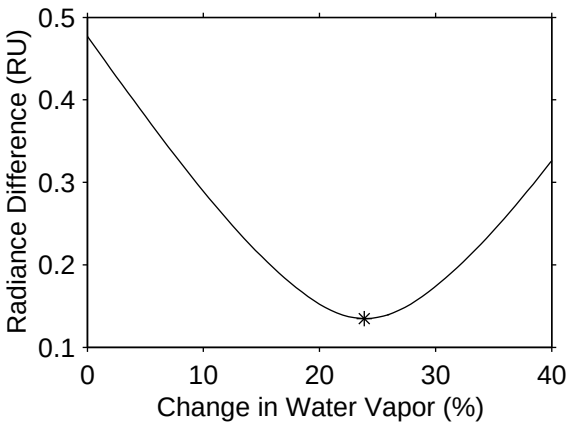

FIG. 5: The RMS difference between measured and simulated downwelling radiances as a function of change in atmospheric water vapor, for 13 January 2004 at 15.4 local time at Dome C. One Radiance Unit (RU) equals 1 mW m^{-2} $(cm^{-1})^{-1}$.

3.3 *Improvement In Agreement between Measured and Simulated Radiances*

Figure 6 shows the difference between simulated and measured downwelling radiances for the afternoon (Fig. 6a) and evening (Fig. 6b) case studies. Differences between simulated and measured radiances are shown near the centers of strong water-vapor lines; the simulated radiances were created using the water-vapor profiles both before the water-vapor correction ("Before Correction", dots) and after ("After Correction", circles). To put the differences near strong water-vapor lines into perspective, the RMS difference (±) for frequencies in the microwindows between strong water-vapor lines is indicated by horizontal dashed lines (the RMS difference for microwindows is insensitive to the water-vapor profile used). Scaling the water-vapor profile reduced the differences at strong line centers to close to the RMS difference for microwindows. The improvement is more dramatic in the afternoon cases (Fig. 6a) than in the evening (Fig. 6b).

3.4 *Error Analysis*

Errors in the measured and simulated downwelling radiances cause errors in the inferred water-vapor scale factor. Some sources of error are random with frequency, such as instrument noise in the PAERI and uncertainty in the effective laser wavenumber, while others may be correlated with frequency, such as nonlinearity of the PAERI detector response to signal, and uncertainties in the temperature and trace gas profiles (Rowe *et al.*, 2006, *in press*; Knuteson *et al.*, 2004a,b).

The uncertainty due to sources of error that are random with frequency can be determined as follows. Referring to Fig. 4, we find the change in water vapor that brings the measured and simulated downwelling

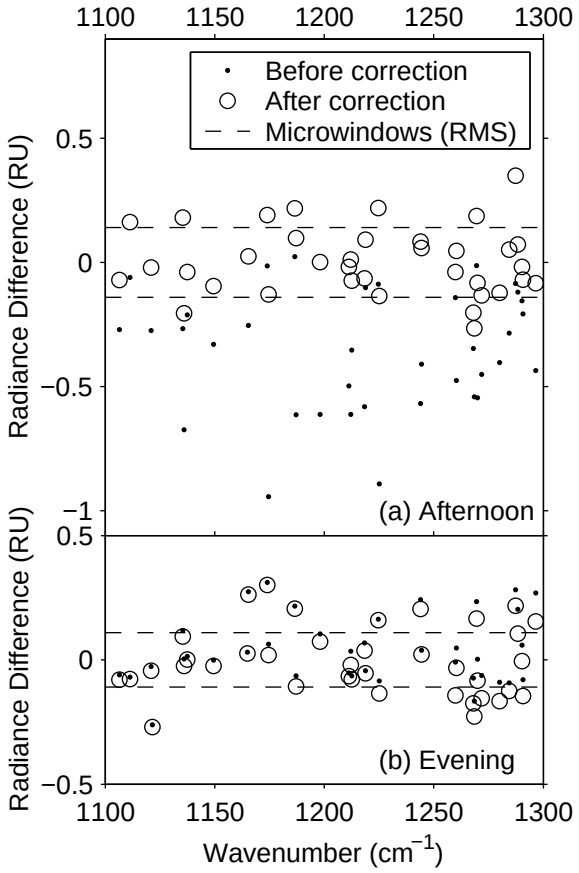

FIG. 6: Simulated minus Measured downwelling radiances for (a) an afternoon dataset and (b) a evening dataset from 13 January 2004 at Dome C. Radiance differences near the centers of strong lines are shown before and after the correction to the water-vapor amount. The RMS radiance difference (±) in the microwindows between strong lines from 1100 to 1300 cm^{-1} is shown for reference (horizontal dashed lines). One Radiance Unit (RU) equals 1 mW m^{-2} $(cm^{-1})^{-1}$.

radiances into agreement at each frequency close to a strong line center. The uncertainty can then be expressed as the standard deviation of the water-vapor changes (Fig. 7). Since approximately 40 frequencies near strong line-centers are used to determine the change in water vapor, the uncertainty in the mean is this standard deviation divided by about 6 (2% in Fig. 7). The uncertainty calculated in this manner was 1-2% for all datasets except 16 January 2004 at 16 LT, which had an uncertainty of 4%.

Sensitivity studies were performed to determine uncertainties in the measured and simulated radiances due to errors that are uncorrelated with frequency as described in Rowe (2005) and Rowe *et al.* (2006, *in press*). These uncertainties were then propagated into uncertainties in the water-vapor correction. The un-

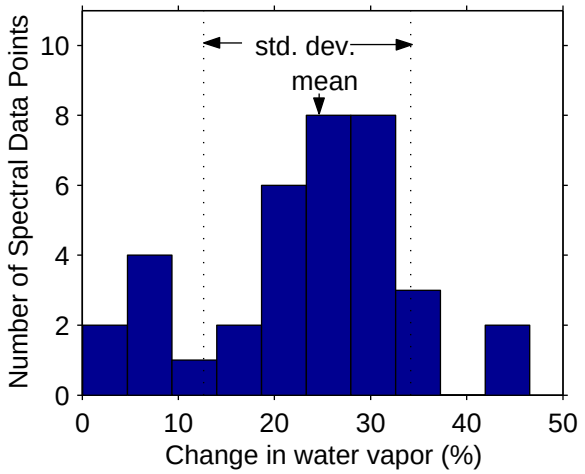

FIG. 7: Occurences of the change in water vapor that minimize the absolute difference between measured and simulated downwelling radiances (13 January 2004 at 15.4 local time). Occurences are spectral frequencies near the centers of strong water-vapor lines between 1100 and 1300 cm^{-1}. The mean and standard deviation (std. dev.) are indicated.

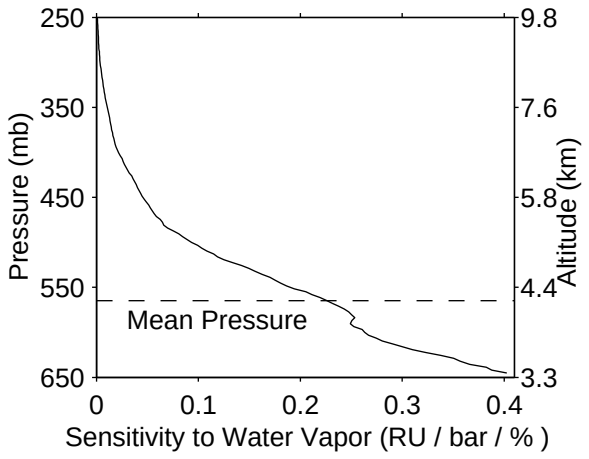

FIG. 8: Sensitivity of the downwelling radiance to a change in water-vapor amount (%) [RU = mW $m^{-2}sr^{-1}(cm^{-1})^{-1}$; bar refers to total pressure], for a typical summertime atmospheric profile over Dome C.

certainty in the temperature profile (0.3 K) depends mainly on limitations in correcting the surface temperature; these are imposed by the measurement accuracy [0.1 mW m^{-2} sr^{-1} $(cm^{-1})^{-1}$, see Knuteson *et al.* (2004a,b)]. Of the trace gases, errors in the concentrations of N_2O and CH_4 have the largest effect on the water-vapor retrieval; each has an uncertainty of 10%. The uncertainties in the water vapor correction due to detector nonlinearity and uncertainties in the temperature profile, trace gas concentrations and the line-shape parameters were 2%, 5%, 2%, 6%, and 0.5%.

The combined uncertainties, including sources of error that are uncorrelated with frequency, are 8-9%.

4. EFFECTIVE ATMOSPHERIC PRESSURE

Emission near strong (but unsaturated) lines of water vapor is influenced by water vapor throughout the troposphere. We determined the sensitivity of the downwelling radiance to fractional changes in water-vapor in atmospheric layers (≈ 3 mb thick). The atmospheric profile used to create the simulated radiance was the average of atmospheric profiles from Dome C datasets. The sensitivity (Fig. 8) was defined to be the change in radiance per percent change in water vapor, per bar of layer thickness. The height coordinate was pressure, rather than altitude, since we are assuming that the dry bias itself is a function of pressure. The mean or effective atmospheric pressure (565 mb; dashed line) is

$$< \mathrm{P} >= \frac{\int_{650}^{0} \mathrm{S(P)PdP}}{\int_{650}^{0} \mathrm{S(P)dP}}. \qquad (2)$$

The mean pressure varied with wavenumber by less than 8 mb. The sensitivity function depends on the atmospheric profile, but is similar for all of our Dome C atmospheres. Our water-vapor correction can then be used to correct the water-vapor amount measured by RS-90 radiosondes in other atmospheres at this effective pressure.

5. RESULTS AND DISCUSSION

Figure 9 shows a profile of water vapor before and after our correction, for the afternoon (Fig. 9a) and evening (Fig. 9b) case studies. The change in water-vapor is considerably greater in the afternoon than evening.

Figure 10 is a histogram showing the water-vapor corrections for all cases used in this study. In the evening (SZAs ≈ 80°), the correction varies from 1% to 13% and in the afternoon (SZAs ≈ 60°), from 13% to 29%. Knowing that each result has an uncertainty of 9%, the combined uncertainties (1 standard deviation) for afternoon and night were calculated using the number of datasets and the student's t. The combined uncertainties (3%) were similar to the standard deviation of the afternoon and of the evening water-vapor corrections (4%). The mean water-vapor correction is 8 ± 3% for the evening, and 23% ± 3% for the afternoon.

Figure 11 shows the water-vapor correction derived by Vőmel *et al.* (2006) for the RS-92 radiosonde (solid), and that determined in this work for SZAs near 60 degrees, for the RS-90 radiosonde (*). The measurements of Vőmel *et al.* were made in the atmosphere

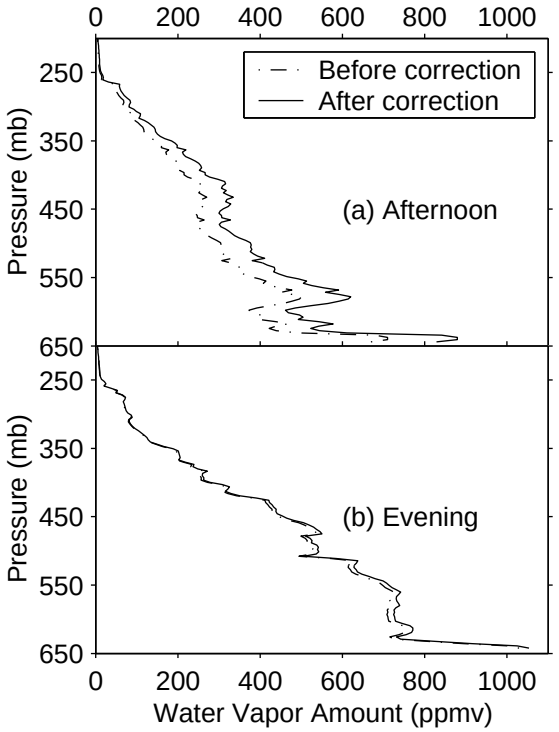

FIG. 9: Profile of water vapor measured by the humidity sensor on the Vaisala radiosonde at Dome C on 13 January 2004 before and after the correction done in this work, for (a) an afternoon measurement set (15.4 local time), and (b) a evening measurement set (23.6 local time).

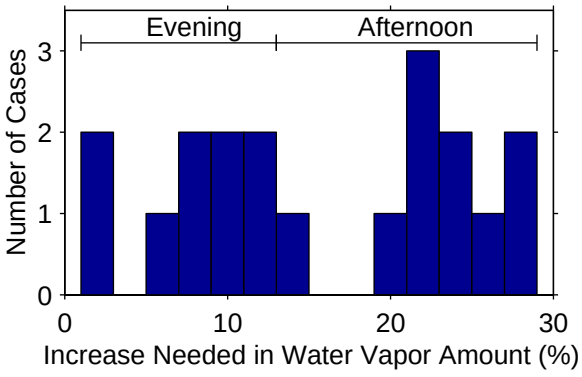

FIG. 10: Increase needed in atmospheric water vapor to obtain best agreement between measured and simulated radiances, for all datasets. The ranges of water-vapor corrections needed for measurements made in the afternoon and evening are indicated.

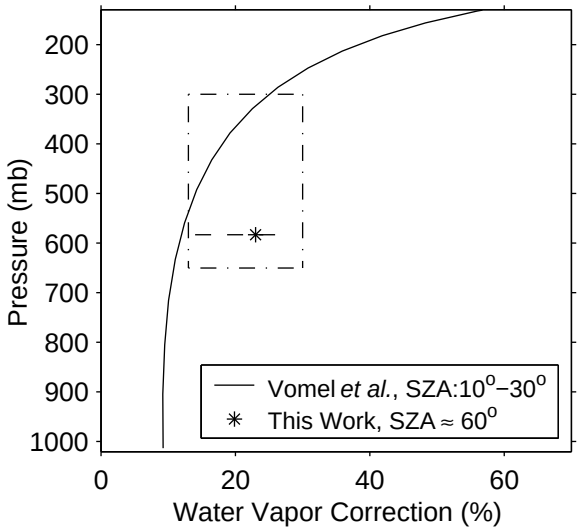

FIG. 11: Correction needed in water-vapor amount as a function of pressure, from Vőmel *et al.* (2006) (solid), and the mean correction determined in this work for solar zenith angles (SZAs) near 60 degrees, at the effective height (star). The dashed box indicates the range of corrections determined and the range of atmospheric pressures influencing the correction.

above Alajuela, Costa Rica at SZAs of 10 to 30 degrees. Our result is shown at the effective pressure of 565 mb. The dashed line indicates the combination of the standard deviation and the average dry bias of the evening datasets, used as an upper limit errors that may be due to sources other than the dry bias caused by solar radiation. The vertical extent of the square (dash-dot) indicates the range of pressures in the Dome C atmosphere important to the correction, while the horizontal extent indicates the range of water-vapor corrections for all afternoon cases. Because the sun is lower in the sky for our measurements, we expect our correction to be less than that of Vőmel *et al.*. In addition, the results of Vőmel *et al.* suggest that the correction needed to the RS-90 humidity is smaller than that needed for the RS-92. Nevertheless, our correction is greater than that of Vőmel *et al.* at 565 mb.

6. CONCLUSIONS

Measurements of downwelling spectral infrared radiance from Dome C, Antarctica are used as a baseline by which to correct Vaisala RS-90 radiosonde humidity profiles. This is done by scaling the radiosonde humidity profiles until the differences in radiance between simulations and the measurements are minimized. We find that the radiosondes are always dry and need to be scaled by about 8% when the SZAs are near 80 degrees and 23% for SZAs near 60 degrees. The corrections derived here correspond to a range of pressures from 650

to 200 mb, or an effective pressure of 565 mb, and can be used to correct RS-90 humidities at other locations at the same pressures and SZAs.

To determine the effect of the dry biases on the tropical outgoing longwave flux in the tropics, we used the tropical standard atmosphere of McClatchey *et al.* (1972). The OLR was calculated at 60 km with LBLRTM, a plane-parallel model. The OLR spectrum was calculated from 0 to 2000 cm^{-1}, for viewing angles from 0 degrees (straight down) to 78 degrees (limb). Assuming azimuthal symmetry, the radiance was numerically integrated over frequency and over solid angle, giving the flux [see Eq. (2) of Town *et al.* (2005)]. Dry biases of 8% and 23% in middle to upper tropospheric humidity in the tropics (650 - 200 mb) result in overestimating outgoing longwave flux by about 1 W m^{-2} and 3 W m^{-2}. Of this, approximately half is due to the dry bias from 650 to 450 mb, and half is from the upper troposphere.

7. ACKNOWLEDGMENTS

We are grateful to the Global Monitoring Division of the Earth System Research Laboratory [formerly the Climate Monitoring and Diagnostics Laboratory (CMDL)] for making their measurements of the concentrations of atmospheric trace gases from South Pole Station available to us. Vital logistical support for our field work at Dome C was provided by the Programma Nazionale di Ricerche in Antartide (PNRA), the Institut Polaire Franais Paul Emile Victor (IPEV), and the Office of Polar Programs at the National Science Foundation. We thank Karim Agabi (U. Nice), Eric Aristidi (U. Nice), Tony Travouillon (U. New South Wales), and W. Lance Roth (U. Idaho) for launching radiosondes at Dome C. This project was supported by NASA grant NAG5-11112.

REFERENCES

Buehler, S. A., V. O. John, A. von Englen, E. Brocard, T. Kuhn and P. Eriksson, 2005: Understanding the global variability of clear-sky outgoing longwave radiation. Submitted to the *Quarterly Journal of Royal Meteorological Society*.

Clough, S. A., R. D. Worsham and M. J. Iacono, 1991: Radiative transfer model development in support of the Atmospheric Radiation Measurement (ARM) program. *Proceedings of the Second Atmospheric Radiation Measurement (ARM) Science Team Meeting*, DOE CONF-9110336.

Conway, T. J., P. P. Tans, L. S. Waterman, K. W. Thoning, D. R. Kitzis, K. A. Masarie and N. Zhang, 1994: Evidence for interannual variability of the carbon cycle from the NOAA/CMDL global air sampling network. *J. Geophys. Res.*, **99**, 22831–22855.

Dlugokencky, E. J., B. P. Walter, K. A. Masarie, P. M. Lang and E. Kasischke, 2001: Measurements of an anomalous global methane increase during 1998. *Geophys. Res. Lett.*, **28**, 499–502.

Hudson, S. R., M. S. Town, V. P. Walden and S. G. Warren, 2004: Temperature, humidity, and pressure response of radiosondes at low temperatures. *J. Atmos. Oceanic Technol.*, pp. 825–836.

Knuteson, R. O., H. E. Revercomb, F. A. Best, N. C. Ciganovich, R. G. Dedecker, T. P. Dirkx, S. Ellington, W. F. Feltz, R. K. Garcia, H. B. Howell, W. L. Smith, J. F. Short and D. C. Tobin, 2004a: Atmospheric Emitted Radiance Interferometer (AERI) Part I: Instrument design. *J. Atmos. Oceanic Technol.*, **21**, 1763–1776.

Knuteson, R. O., H. E. Revercomb, F. A. Best, N. C. Ciganovich, R. G. Dedecker, T. P. Dirkx, S. Ellington, W. F. Feltz, R. K. Garcia, H. B. Howell, W. L. Smith, J. F. Short and D. C. Tobin, 2004b: Atmospheric Emitted Radiance Interferometer (AERI) Part II: Instrument performance,. *J. Atmos. Oceanic Technol.*, **21**, 1777–1789.

McClatchey, R. A., R. W. Fenn, J. E. A. Selby, F. E. Volz and J. S. Garing, 1972: Optical properties of the atmosphere (third edition). *Air Force Geophysical Laboratories report, AFCRL-72-0497*, **108**.

Miloshevich, L. M., A. Paukkunen, H. Vőmel and S. J. Oltmans, 2004: Development and validation of a time-lag correction for Vaisala radiosonde humidity measurements. *J. Atmos. Oceanic Technol.*, **21**, 1305–1327.

Miloshevich, L. M., H. Vőmel, A. Paukkunen, A. J. Heymsfield and S. J. Oltmans, 2001: Characterization and correction of relative humidity measurements from Vaisala RS80-A radiosondes at cold temperatures. *J. Atmos. Oceanic Technol.*, **18**, 135–156.

Miloshevich, L. M., H. Vőmel, D. N. Whiteman, B. M. Lesht, F. J. Schmidlin and F. Russo, 2006: Absolute accuracy of water vapor measurements from six operational radiosonde types launched during AWEX-G, and implications for AIRS validation. *Journal of Geophysical Research*, **111**.

NOAA-CMDL, 2000: National Oceanic and Atmospheric Administration - Climate Monitoring and Diagnostics Lab (NOAA-CMDL). http://www.cmdl.noaa.gov.

Novelli, P. C., J. E. Elkins and L. P. Steele, 1991: The development and evaluation of a gravimetric reference scale for measurements of atmospheric carbon monoxide. *J. Geophys. Res.*, **96**(13), 109–13,121.

Rothman, L. S., A. Barbe, D. C. Benner, L. R. Brown, C. Camy-Peyret, M. R. Carleer, K. Chance, C. Clerbaux, V. Dana, V. M. Devi, A. Fayt, J. M. Flaud,

R. R. Gamache, A. Goldman, D. Jacquemart, K. W. Jucks, W. J. Lafferty, J. Y. Mandin, S. T. Massie, V. Nemtchinov, D. A. Newnham, A. Perrin, C. P. Rinsland, J. Schroeder, K. M. Smith, M. A. H. Smith, K. Tang, R. A. Toth, J. Vander Auwera, P. Varanasi and K. Yoshino, 2003: The HITRAN molecular spectroscopic database: edition of 2000 including updates through 2001. *J. Quant. Spect. Radiat. Trans. (JQSRT)*, **82**, 5–44.

Rowe, P. M., 2004: *Measurements of the Foreign-Broadened Continuum of Water Vapor in the 6.3 micron band at -30 Celsius*. Ph.D. thesis, University of Washington, Seattle, Washington.

Rowe, P. M., V. P. Walden and S. G. Warren, 2006: Measurements of the foreign-broadened continuum of water vapor in the 6.3-mm band at -30°C. *Applied Optics*, *in press*.

Sinha, A. and J. E. Harries, 1995: Water vapor and greenhouse trapping: The role of far infrared absorption. *Geophysical Research Letters*, **22**, 2147–2150.

Town, M. S., V. P. Walden and S. G. Warren, 2005: Spectral and broadband longwave downwelling radiative fluxes, cloud radiative forcing, and fractional cloud cover over the south pole. *American Meteorological Society*, pp. 4235–4252.

Turner, D. D., B. M. Lesht, S. A. Clough, J. C. Liljegren, H. E. Revercomb and D. C. Tobin, 2003: Dry bias and variability in Vaisala RS80-H radiosondes: The ARM experience. *J. Atmos. Oceanic Technol.*, **20**, 1560–1567.

Vőmel, H., H. Selkirk, J. Valverde-Canossa, J. Valdés, E. Kyrő, R. Kivi, W. Stolz, G. Peng and J. A. Diaz, 2006: Radiation dry bias of the Vaisala RS92 humidity sensor. *J. Atmos. Oceanic Technol.*, **submitted**.

Walden, V. P., S. G. Warren and F. J. Murcray, 1998: Measurements of the downward longwave radiation spectrum over the Antarctic plateau and comparisons to a line-by-line radiative transfer model for clear skies. *J. Geophys. Res.*, **103**, 3825–3846.

Wang, J., H. L. Cole, D. J. Carlson, E. R. Miller, K. Beierle, A. Paukkunen and T. K. Laine, 2002: Corrections of humidity measurement errors from the Vaisala RS80 radiosonde - application to TOGA COARE data. *J. Atmos. Oceanic Technol.*, **19**, 981–1002.